An Analytical Solution for Deformation of Underground Openings Excavated in Fractured Rocks

Amir R. Khoshboresh, M.Sc., P.Eng.
DST Consulting Engineers Inc., A Division of Englobe, Sudbury, ON, Canada

ABSTRACT
Excessive deformation of rock mass around underground openings are frequently encountered in mines and underground structures. It is particularly common in the tunnels excavated in soft rocks, the rock masses subjected to high in-situ stresses, and the weak rock masses that have been heavily sheared. Conventional approaches in the estimation of deformation in tunnels, such as Sulem et al. (1987), assumed that the tunnel is deep enough to consider that the stress distribution is homogeneous. However, in most cases in practice, the stress distribution around the tunnels are not homogeneous and isotropic. New correlations are therefore developed as part of this study[1] to generalize the Sulem et al. equations by considering a non-homogeneous stress distribution (biaxial stress field) around the tunnel. The comparative results showed although the numerical results are very close to the analytical solution results, there is still a significant difference between the field data and analytical results.

RÉSUMÉ
Des déformations excessives de masse rocheuse autour des ouvertures souterraines sont fréquemment rencontrées dans les mines et les structures souterraines. Il est particulièrement commun dans les tunnels creusés dans des roches tendres, dans les masses rocheuses soumises à de fortes contraintes in situ et dans les masses rocheuses faibles fortement cisaillées. Les approches conventionnelles dans l'estimation de la déformation dans les tunnels, tel que Sulem et al. (1987), supposent que le tunnel est suffisamment profond pour considérer que la répartition des contraintes est homogène. Cependant, dans la plupart des cas, la répartition des contraintes autour des tunnels n'est ni homogène ni isotrope. De nouvelles corrélations sont donc développées dans le cadre de cette étude pour généraliser les relations de Sulem et al. équations en considérant une non homogène répartition des contraintes (champ de contraintes biaxiales) autour du tunnel. Les résultats comparatifs ont montré que, bien que les résultats numériques soient très proches des résultats de la solution analytique, il existe toujours une différence significative entre les données de terrain et les résultats analytiques.

1 INTRODUCTION

Excessive deformation of rock mass around underground openings is frequently encountered in the mines and underground structures. It is particularly common in the tunnels excavated in soft rocks, the rock masses subjected to high in-situ stresses, and the weak rock masses, which have been heavily sheared. The excessive deformation in fault and shear fractured zones is one of the difficulties that is frequently encountered in the construction of the long tunnels and sometimes leads to failure of supporting systems and collapse in tunnels. Potential localized failure and/or collapse in tunnels will incur a significant additional cost, extended schedule, and safety risks on the projects.

Evaluating actual deformation of rock mass in underground openings requires knowledge of the rock-support interaction and careful interpretation of field data, simultaneously. The main purpose of monitoring of the tunnels during construction was primarily to measure the ground pressures acting on the support systems. However, the modern tunnelling technologies emphasize monitoring of observed displacements during and after the construction of the tunnels. Nowadays, advanced design and construction methods, such as the New Austrian Tunnelling Method (NATM), are also being applied to avoid the excessive deformations of rock mass around the tunnels and underground openings.

2 PROBLEM STATEMENT

Conventional approaches in estimation of deformation in tunnels, such as Sulem et al. (1987), assumed that the tunnel has a circular cross-section and around the tunnel, the rock is homogeneous and isotropic, and also the tunnel is deep enough to consider that the stress distribution around the tunnel is homogeneous (hydrostatic). However, in most cases in practice, the stress distribution around the tunnels is not homogeneous and isotropic.

New correlations are therefore developed as part of this study to generalize Sulem et al. equations by considering a non-homogeneous stress distribution (biaxial stress field) around the tunnel.

3 GENERALIZED SULEM EQUATIONS

3.1 Estimation of induced stresses around an opening using Kirsch equations

In order to calculate stresses, strains and displacements induced around underground openings in the elastic materials, it is necessary to use the mathematical theory of elasticity. This requires a set of equilibrium and displacement compatibility equations to be solved for given boundary conditions and constitutive equations for the

1. This study is part of a Master Thesis, which was completed at Laval University Research Center in underground support systems.

elastic materials. The process involved in obtaining the required solutions can become entirely complex and tedious.

One of the earliest solutions for the two-dimensional distribution of stresses around an opening in an elastic media was published by Kirsch (1898) for the simplest cross-sectional shape, the circular hole. A full discussion on the derivation of the Kirsch equations, as they are known now, is given by Jaeger and Cook (1969). Figure 1 demonstrates a system of polar coordinates for Kirsch equations that stresses are defined in terms of the tractions acting on the faces of an element located by a radius ρ and a polar angle θ.

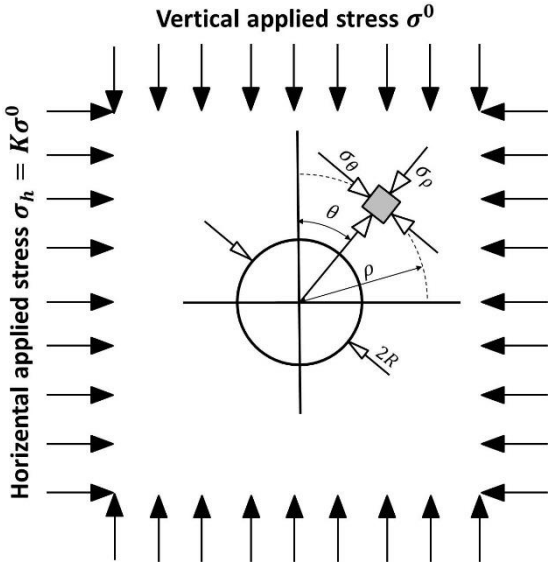

Figure 1. Two-dimensional distribution of stresses around an opening in non-hydrostatic stress field (biaxial)

As per the Kirsch equations, the radial and tangential stress components at point (ρ, θ) can be presented as follows (respectively):

$$\sigma_\rho = \frac{1}{2}\,\sigma^0\,[(1+K)\left(1-\frac{R^2}{\rho^2}\right) +(1-K)\left(1-4\frac{R^2}{\rho^2}+3\frac{R^4}{\rho^4}\right)cos\,2\theta] \quad [1]$$

$$\sigma_\theta = \frac{1}{2}\,\sigma^0\,[(1+K)\left(1+\frac{R^2}{\rho^2}\right) -(1-K)\left(1+3\frac{R^4}{\rho^4}\right)cos\,2\theta] \quad [2]$$

where σ_ρ is the radial stress and σ_θ is the tangential stress at point (ρ, θ).

3.2 Fictitious Support Pressure Coefficient (λ) for Non-hydrostatic Condition

As per Sulem et al. (1987), in the plane-strain problem, the induced radial stress σ_ρ and tangential stress σ_θ applied on the tunnel wall can be obtained using the following equations:

$$\sigma_\rho = (1-\lambda)\,\sigma^0 \quad [3]$$

$$\sigma_\theta = (1+\lambda)\,\sigma^0 \quad [4]$$

where σ^0 is the initial stress in a hydrostatic stress field and λ is defined as fictitious support pressure coefficient. As shown in Figure 2, the radial stress on the tunnel wall is decreased from an initial value equal to the initial stress σ^0, where $\lambda = 0$, to zero in case of no support, where $\lambda = 1$.

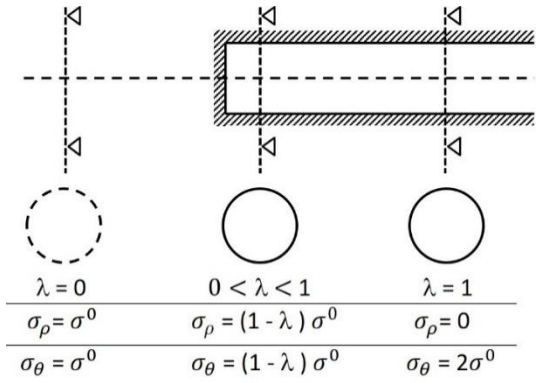

Figure 2: Sulem fictitious support pressure coefficient

Also, the tangential stress on the tunnel wall is decreased from an initial value equal to σ^0, where $\lambda = 0$, to two times of initial stress ($2\sigma^0$) in case of no support, where $\lambda = 1$. In the plane-strain problem for a non-hydrostatic stress field conditions, it was assumed that the radial and tangential stresses in Kirsch equations simulate this face effect and this fictitious temporary support is given by:

$$\sigma_\rho = \frac{1}{2}\,\sigma^0\,[(1+K)(1-\lambda\frac{R^2}{\rho^2}) +(1-K)(1-4\lambda\frac{R^2}{\rho^2}+3\lambda\frac{R^4}{\rho^4})\,cos\,2\theta] \quad [5]$$

$$\sigma_\theta = \frac{1}{2}\,\sigma^0\,[(1+K)(1+\lambda\frac{R^2}{\rho^2}) -(1-K)(1+3\lambda\frac{R^4}{\rho^4})\,cos\,2\theta] \quad [6]$$

where the parameter λ is increased from 0 to 1. Therefore, the radial stress σ_ρ and the tangential stress σ_θ applied on the tunnel wall ($\rho = R$) in case of no support can be presented as follows:

$$\sigma_\rho = \frac{1}{2}\,\sigma^0\,[(1+K)(1-\lambda) + (1-K)(1-\lambda)\,cos\,2\theta] \qquad [7]$$

$$\sigma_\theta = \frac{1}{2}\,\sigma^0\,[(1+K)(1+\lambda) - (1-K)(1+3\lambda)\,cos\,2\theta] \qquad [8]$$

As per the recent equations, in the roof and bottom of the tunnel, where θ = 0° and θ = 180°, respectively, Eqs. 7 and 8 can be presented as follows:

$$\sigma_\rho = (1-\lambda)\sigma^0 \qquad [9]$$

$$\sigma_\theta = [K - (1-2K)\lambda]\sigma^0 \qquad [10]$$

In addition, in sidewalls of the tunnel, where θ = 90° and θ = 270°, the induced stresses components are given by:

$$\sigma_\rho = K(1-\lambda)\,\sigma^0 \qquad [11]$$

$$\sigma_\theta = [1 - (K-2)\lambda]\,\sigma^0 \qquad [12]$$

Furthermore, in particular case K = 0, Eqs. 5 and 6 can be presented as follows:

$$\sigma_\rho = \frac{1}{2}\,\sigma^0\,[\left(1 - \lambda\frac{R^2}{\rho^2}\right) + \left(1 - 4\lambda\frac{R^2}{\rho^2} + 3\lambda\frac{R^4}{\rho^4}\right)cos\,2\theta] \qquad [13]$$

$$\sigma_\theta = \frac{1}{2}\,\sigma^0\,\left[\left(1 + \lambda\frac{R^2}{\rho^2}\right) - \left(1 + 3\lambda\frac{R^4}{\rho^4}\right)cos\,2\theta\right] \qquad [14]$$

and in the hydrostatic stress field (K = 1), Eqs. 5 and 6 can be presented as follows:

$$\sigma_\rho = \left(1 - \lambda\frac{R^2}{\rho^2}\right)\sigma^0 \qquad [15]$$

$$\sigma_\theta = \left(1 + \lambda\frac{R^2}{\rho^2}\right)\sigma^0 \qquad [16]$$

As shown in the recent Eqs. 15 and 16, in a hydrostatic stress field, the radial and tangential stress components are independent of θ. Therefore, the radial and tangential stress components around the tunnel walls ($\rho = R$) in a hydrostatic stress field are given by:

$$\sigma_\rho = (1-\lambda)\sigma^0$$

$$\sigma_\theta = (1+\lambda)\sigma^0$$

The recent equations are indeed the Sulem et al. (1987) equations (Eqs. 3 and 4), which were already presented. The ratio of sidewall radial and tangential stresses to vertical applied stress (σ_ρ/σ^0 and σ_θ/σ^0) against the ratio of radial distance to the radius of the tunnel (ρ/R) were plotted for two special cases K = 0 and K = 1 and presented in Figure 3.

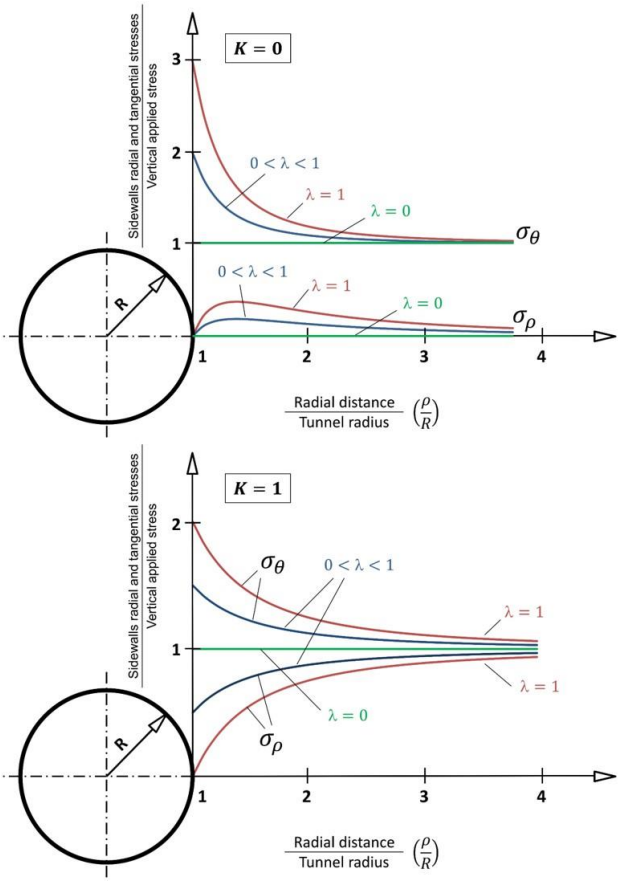

Figure 3. Distributions of sidewalls radial and tangential stresses in case K = 0 and K = 1

The distribution of stresses in Figure 3 shows that the tangential stress gradually decreases to the value of vertical stress in an approximate distance of $\rho = 4R$. This fact is being applied now to set up the numerical models for tunnels and underground openings. Generally, it is

recommended that the dimensions of the numerical model be considered greater than 4 times the tunnel radius, approximately.

The radial stress components in Eqs. 9 and 11 were also plotted and presented in Figure 4. As shown, the radial stress is independent of K in the roof and bottom of the tunnel. In addition, the radial stress is equal to zero in the case of λ = 1.

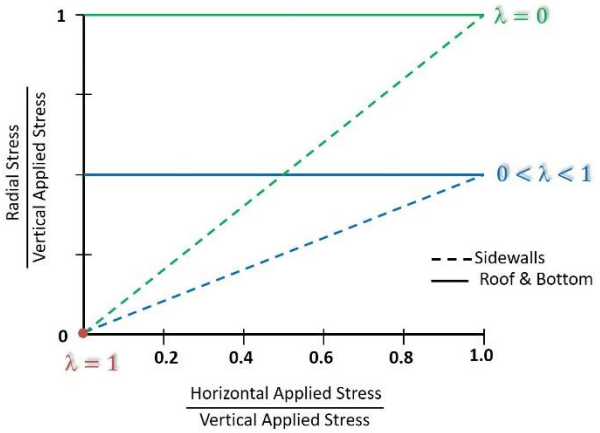

Figure 4. Variation of radial stress in sidewalls and roof & bottom of the tunnel against K

Moreover, the tangential stress component in Eqs. 10 and 12 were plotted and presented in Figure 5.

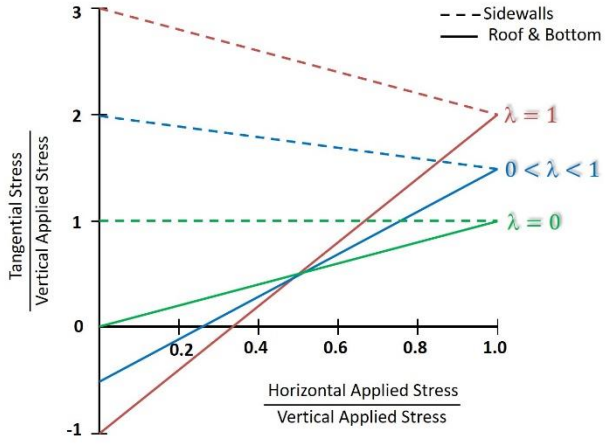

Figure 5. Variation of tangential stress in sidewalls and roof & bottom of the tunnel against K

As shown in Figure 5, by increasing K, the tangential stress increases in the roof and bottom of the tunnel and decreases in the sidewalls. However, in the case of λ = 0, the tangential stress is equal to the vertical applied stress (initial stress).

3.3 Generalized Sulem Equations for Non-hydrostatic Condition Using Generalized Hoek-Brown Criterion

As long as λ is smaller than a certain value λ_e, the yield criterion is not reached at any point of the rock mass. The parameter λ_e is defined as value of the parameter λ when the yield criterion is reached at the tunnel wall. When $\lambda = \lambda_e$ the yield criterion is reached at $\rho = R$, the elastic stresses at the roof and bottom of the tunnel must then also satisfy the yield criterion. Using the generalized Sulem equations in roof and bottom of the tunnel (Eqs. 9 and 10):

$$\sigma_\rho = (1-\lambda_e)\,\sigma^0 \qquad [17]$$

$$\sigma_\theta = [K-(1-2K)\lambda_e]\,\sigma^0 \qquad [18]$$

Therefore, using the generalized Hoek-Brown criterion:

$$\sigma_\theta = \sigma_r + \sigma_{ci}\left(m_b\,\frac{\sigma_r}{\sigma_{ci}} + s\right)^a$$

$$[K-(1-2K)\lambda_e]\,\sigma_v = (1-\lambda_e)\,\sigma_v + \sigma_{ci}(m_b\,\frac{(1-\lambda_e)\,\sigma_v}{\sigma_{ci}} + s)^a$$

It was assumed a = 0.5 since the parameter a in generalized Hoek-Brown failure criterion for most of the rocks is close to 0.5, therefore:

$$[K-(1-2K)\lambda_e]\,\sigma_v = (1-\lambda_e)\,\sigma_v + \sigma_{ci}(m_b\,\frac{(1-\lambda_e)\,\sigma_v}{\sigma_{ci}} + s)^{0.5}$$

Solving the recent quadratic equation, the parameter λ_e for roof and bottom of the tunnel is given by:

$$\lambda_e = \{[(4K(K-1)\sigma_v{}^2 + m_b\sigma_{ci}\sigma_v)^2 - 16K^2\sigma_v{}^2((K-1)^2\sigma_v{}^2 - m_b\sigma_{ci}\sigma_v - s\sigma_{ci}{}^2)]^{0.5} - [4K(K-1)\sigma_v{}^2 + m_b\sigma_{ci}\sigma_v]\}/8K^2\sigma_v{}^2 \qquad [19]$$

Also, the elastic stresses at sidewalls of the tunnel must satisfy the yield criterion. Using the generalized Sulem equations in sidewalls of the tunnel (Eqs. 11 and 12):

$$\sigma_r = K(1-\lambda_e)\,\sigma_v \qquad [20]$$

$$\sigma_\theta = [1-(K-2)\lambda_e]\,\sigma_v \qquad [21]$$

$$[1-(K-2)\lambda_e]\,\sigma^0 = K(1-\lambda_e)\,\sigma^0 + \sigma_{ci}(m_b\,\frac{K(1-\lambda_e)\,\sigma^0}{\sigma_{ci}} + s)^{0.5}$$

Therefore, with the same approach and solving the recent quadratic equation, the parameter λ_e for sidewalls of the tunnel is given by:

$$\lambda_e = \{[(4(1-K)\sigma_v{}^2 + Km_b\sigma_{ci}\sigma_v)^2 - 16\sigma_v{}^2((1-K)^2\sigma_v{}^2 - Km_b\sigma_{ci}\sigma_v - s\sigma_{ci}{}^2)]^{0.5} - [4(1-K)\sigma_v{}^2 + Km_b\sigma_{ci}\sigma_v]\}/8\sigma_v{}^2 \quad [22]$$

For $\lambda > \lambda_e$ a broken zone of radius r_p will develop around the tunnel. It was assumed the equation of equilibrium is valid around the tunnel in this condition:

$$\frac{\delta\sigma_r}{\delta r} = \frac{\sigma_\theta - \sigma_r}{r} \quad [23]$$

Within the broken zone, the equation of equilibrium is integrated by substituting the non-linear Generalized Hoek-Brown failure criterion with respect to the boundary conditions:

$$\frac{\delta r}{r} = \frac{\delta\sigma_r}{(m_b\,\sigma_v\,\sigma_r + s\sigma_{ci}{}^2)^{0.5}}$$

The boundary conditions in the roof and bottom of the tunnel are defined as follows:

$$\begin{cases}\sigma_\rho(R,t) = [1-\lambda(t)]\,\sigma^0\\ \sigma_\rho(r_b(t),t) = [1-\lambda_e]\,\sigma^0\end{cases} \quad [24]$$

therefore:

$$\int_R^\rho \frac{\delta\rho}{\rho} = \int_{\sigma_\rho(r,t)}^{\sigma_\rho(r_d(t),t)} \frac{\delta\sigma_\rho}{\sigma_\theta - \sigma_\rho} = \int_{\sigma_\rho(r,t)}^{\sigma_\rho(r_d(t),t)} \frac{\delta\sigma_\rho}{\left(m_b\,\sigma_{ci}\,\sigma_\rho + s\sigma_{ci}{}^2\right)^{0.5}}$$

$$\ln\left(\frac{\rho}{r}\right) = \left[\frac{2\left(m_b\,\sigma_{ci}\,\sigma_\rho + s\sigma_{ci}{}^2\right)^{0.5}}{m_b\,\sigma_{ci}}\right]_{[1-\lambda(t)]\,\sigma^0}^{\sigma_\rho}$$

then:

$$\sigma_\rho = \frac{m_b\,\sigma_{ci}}{4}\left[\ln\left(\frac{\rho}{r}\right)\right]^2 + \ln\left(\frac{\rho}{r}\right)\{m_b\,\sigma_{ci}\,\sigma^0\,[1-\lambda(t)] + s\sigma_{ci}{}^2\}^{0.5} + [1-\lambda(t)]\,\sigma^0 \quad [25]$$

Also, the boundary conditions in the sidewalls of the tunnel are defined as follows:

$$\begin{cases}\sigma_\rho(R,t) = K[1-\lambda(t)]\,\sigma^0\\ \sigma_\rho(r_b(t),t) = K[1-\lambda_e]\,\sigma^0\end{cases} \quad [26]$$

therefore:

$$\int_R^\rho \frac{\delta\rho}{\rho} = \int_{\sigma_\rho(r,t)}^{\sigma_\rho(r_d(t),t)} \frac{\delta\sigma_\rho}{\sigma_\theta - \sigma_\rho} = \int_{\sigma_\rho(r,t)}^{\sigma_\rho(r_d(t),t)} \frac{\delta\sigma_\rho}{\left(m_b\,\sigma_{ci}\,\sigma_\rho + s\sigma_{ci}{}^2\right)^{0.5}}$$

$$\ln\left(\frac{\rho}{r}\right) = \left[\frac{2\left(m_b\,\sigma_{ci}\,\sigma_\rho + s\sigma_{ci}{}^2\right)^{0.5}}{m_b\,\sigma_{ci}}\right]_{K[1-\lambda(t)]\,\sigma^0}^{\sigma_\rho}$$

then:

$$\sigma_\rho = \frac{m_b\,\sigma_{ci}}{4}\left[\ln\left(\frac{\rho}{r}\right)\right]^2 + \ln\left(\frac{\rho}{r}\right)\{m_b\,\sigma_{ci}\,\sigma^0\,K[1-\lambda(t)] + s\sigma_{ci}{}^2\}^{0.5} + K[1-\lambda(t)]\,\sigma^0 \quad [27]$$

The radius of the broken zone can be calculated by considering the continuity of the radial stress field across the elastoplastic boundary. In the roof and bottom of the tunnel:

$$ln\left(\frac{r_P}{r}\right) = \{2\{[m_b\,\sigma_{ci}\,\sigma^0\,[1-\lambda(t)] + s\sigma_{ci}{}^2] - m_b\,\sigma_{ci}\left[[1-\lambda(t)]\,\sigma^0 - \sigma_{\rho_P}\right]\}^{0.5} - 2\{m_b\,\sigma_{ci}\,\sigma^0\,[1-\lambda(t)] + s\sigma_{ci}{}^2\}^{0.5}\}/m_b\,\sigma_{ci} \quad [28]$$

where σ_{ρ_P} is the radial stress in elastoplastic boundary:

$$\sigma_{\rho_P} = [1-\lambda_e]\,\sigma^0 \quad [29]$$

Also, the radius of the broken zone in sidewalls of the tunnel can be given by:

$$ln\left(\frac{r_P}{r}\right) = \{\, 2\{[m_b\, \sigma_{ci}\, \sigma^0\, K[1-\lambda(t)] + s\sigma_{ci}{}^2]$$

$$-m_b\, \sigma_{ci}\big[K[1-\lambda(t)]\, \sigma^0 - \sigma_{\rho_P}\big]\}^{0.5}$$

$$-2\{m_b\, \sigma_{ci}\, \sigma^0\, K[1-\lambda(t)] + s\sigma_{ci}{}^2\}^{0.5}\}/m_b\, \sigma_{ci} \qquad [30]$$

However, similar to the Sulem et al. (1987) approach, the radial displacement around the tunnel at $\rho = r$ is given by:

$$\frac{u_r}{r} = \lambda_e \frac{\sigma^0}{2G_0}\left(\frac{r_P}{r}\right)^2 \left[1 + \frac{G_0}{G_f}\, f(t)\right] \qquad [31]$$

$\lambda_e \frac{\sigma^0}{2G_0}\left(\frac{r_P}{r}\right)^2$: depends only on the face advance effect

$1 + \frac{G_0}{G_f}\, f(t)$: depends only on the creep effect

where G_0, G_f, and $f(t)$ are shear modulus, creep modulus, and creep function, respectively.

4 VALIDATION OF DEVELOPED ANALYTICAL SOLUTION

4.1 Case Study and Field Data

Seimare dam & hydroelectric power plant was constructed on Seimare River in the southwest of Iran. The project is included a double arc concrete dam with 180 m height and a power plant with 3 units of 160 megawatts, located about 2.5 km downstream side of the dam. The required water is supplied to the power plant through a 1476 m long power tunnel (diameter 11 m) and three 170 m long penstock tunnels (average diameter 5.7 m). There is also a 71 m high vertical shaft (diameter 8 m) and a surge tank (diameter varying from 40 to 77.75 m) located in 1350 m distance from the inlet structure of the power tunnel (Figure 6).

For monitoring of the Seimare Power Tunnel, several stations were installed during construction of the tunnel. In this study, only the collected field data from two monitoring stations (section B-B in chainage of 0+350.50 km and section D-D in chainage of 1+041.50 km) were used. Figure 6 also demonstrates the location of the stations along the power tunnel. The overburden in the monitoring stations of B-B and D-D was calculated at 184.9 and 178.3 m, respectively.

Convergence meter (three reference points) was used to measure the displacements around the tunnel. The monitoring program results showed a positive trend in the displacement curve with a low rate of displacement. Also, the obtained results during a period of 100 days for two stations showed that the convergence of the tunnel sidewalls was stabilized after about 30 days. The maximum values of the tunnel convergence for two stations are presented in Table 2.

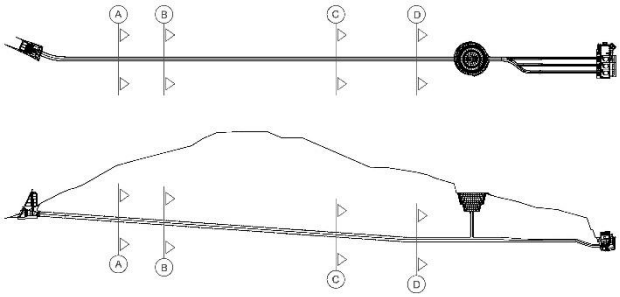

Figure 6. Monitoring station locations along power tunnel

The maximum displacements were recorded at 41 and 28 mm in sidewalls of the sections B-B and DD, respectively. In comparison with sidewall displacements, the maximum displacements in the roof of the tunnel in both stations were negligible, indicating horizontal initial stress bigger than vertical initial stress (K > 1) in both stations.

Table 2. Maximum values of tunnel convergence in two stations (from monthly Seimare monitoring reports, 2003)

Section	Chainage (km)	Overburden thickness (m)	Disp* 1-2	Disp 2-3	Disp 3-1
B-B	0+350.5	184.9	8	41	5
D-D	1+041.5	178.3	6	28	3

* Disp: Displacement (mm)

4.2 Numerical Modelling and Deformation Analysis

Several numerical models were set up and ran using COMSOL Multiphysics finite elements software to compare with the proposed analytical solution and collected field data. The numerical analyses were conducted for two general conditions; time-dependent and time-independent conditions. A 12 m diameter circular tunnel was considered to be modelled. Given that the problem is symmetric, a quarter of the tunnel with 7932 triangular meshing elements was considered to be simulated.

As per available background field information (second phase and complementary studies reports), the power tunnel was advanced through the Ravandi anticline and therefore the stresses distribution around the tunnel was considered as a function of overburden and other geotectonics and geomechanical forces in this region. However, the ratio of horizontal applied stress to vertical applied stress (K) was determined at 1.2 and 1.1 in the stations B-B and D-D, respectively. Table 3 summarizes some of the geotechnical properties of the rock mass, which were used in this analysis.

Table 3. Geotechnical properties used in modelling

Property	Unit	Quantity
Modulus of Elasticity (*E*)	GPa	9
Poisson's ratio (ν)	Unitless	0.3
Density (ρ)	Kg/m^3	2600
Cohesion (*C*)	MPa	0.5
Internal Friction Angle (ϕ)	Degree	35

A time-dependent numerical analysis was carried out for a duration of 100 days for two sections. Figure 7 demonstrates the horizontal displacements (X component) within the tunnel sidewall for two sections in time-dependent conditions. In addition, the radius of plastic zones was calculated at 7.9 and 7.8 m (from the central point of the tunnel) for stations B-B and D-D, respectively.

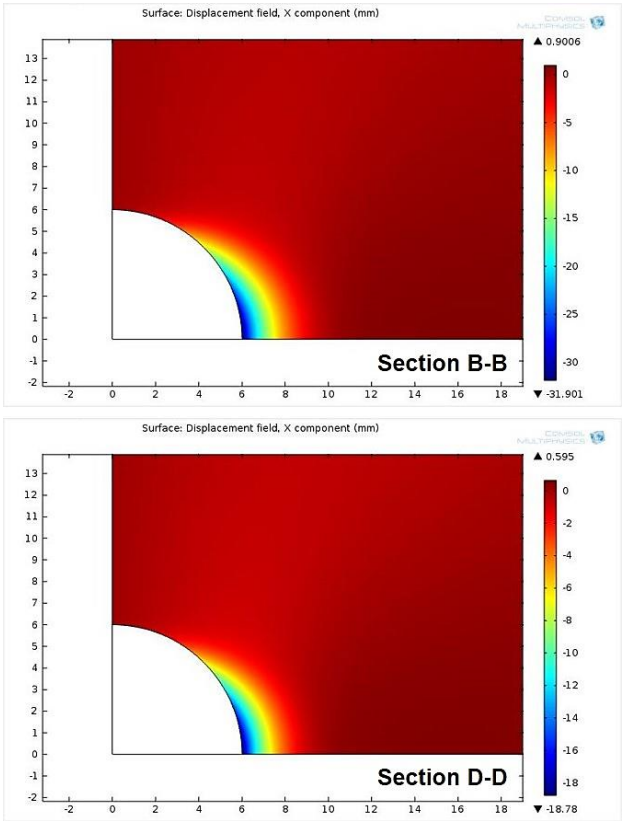

Figure 7. Horizontal displacements (X component) in the tunnel sidewall in time-dependent conditions (mm)

4.3 Analytical Solution Results

Since the Seimare power tunnel has been driven in the jointed/fractured rocks, the generalized Hoek-Brown failure criterion (non-linear) was used in this study. Given that a controlled blasting method was performed during the excavation of the tunnel to prevent damage to surrounding rock mass, the disturbance factor D of generalized Hoek-Brown failure criterion was assumed at 0.7 (good blasting). Using geological and rock mechanics reports for Seimare power tunnel (second phase and complementary studies), the Hoek-Brown parameters σ_{ci}, GSI, and m_i for the rock mass were adopted at 48.3, 55 and 13.5, respectively. Based on the adopted parameters, the other Hoek-Brown parameters a, s, and m_b were calculated at 0.5, 0.00147, and 1.14, respectively.

Using Eq. 19, the values of λ_e in the roof and bottom of the power tunnel ($\theta = 90^o$ and $\theta = 270^o$) are summarized in Table 4. Also, Table 4 shows the values of λ_e in sidewalls of the power tunnel ($\theta = 0^o$ and $\theta = 180^o$), according to Eq. 22, for two stations.

Table 4. Value of λ_e around of the power tunnel

Location	Section B-B	Section D-D
Roof & Bottom	0.8213	0.7940
Sidewalls	0.8102	0.7887

In addition, the radius of the broken zone (plastic region) in the roof and bottom of the power tunnel was calculated using Eq. 28 and presented in Table 5. The radius of the broken zone within the sidewalls of the power tunnel was also calculated using Eq. 30 and presented in Table 5.

Table 5. Value of r_P around the power tunnel (m)

Location	Section B-B	Section D-D
Roof & Bottom	6.29	6.54
Sidewalls	8.19	7.84

The creep function in Eq. 31 was assumed as follows:

$$f(t) = 1 - [T/(t+T)]^m \qquad [32]$$

Using Eq. 31 and considering T=0.2 days and m = 0.15, the radial displacement in the sidewall of the tunnel ($\rho = R$) was calculated for a duration of 100 days.

4.4 Comparison of Obtained Results

Figure 8 compares the collected field data from the monitoring program with the numerical and analytical results. The comparative results showed although the numerical results were very close to the analytical results, there is still a significant difference between the field data and analytical results. However, such differences were predictable since the influence of other construction activities such as excavation of shaft (vertical tunnel and surge tank) and power station as well as the power tunnel from another side, which were under construction at the same time, were not considered in the modelling and numerical analysis and analytical solution.

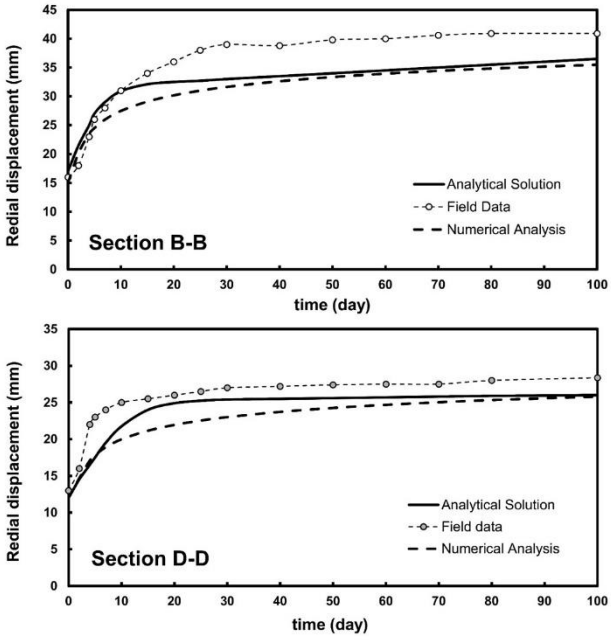

Figure 8. Comparison between the experimental data (monitoring), numerical analysis (FEM) and analytical solution

Obviously, such construction activities probably affected on the deformation of the power tunnel during construction and consequently on the results of monitoring.

On the other hand, the initial data (geotechnical parameters) that were used in numerical analysis and analytical solution for the selected sections, such as Hoek-Brown criterion parameters and ratio of horizontal stress to vertical stress (K), probably did not have required accuracy, since they are extracted as a general representative of the rock mass in this region, not for a particular section of the power tunnel.

5 CONCLUSION

Time-dependent deformations in a rock mass may be manifested as creep of the intact material or creep along the discontinuities.

In the case of a circular tunnel driven through a homogeneous isotropic linear visco-elastic medium, Sulem et al. (1987) presented an analytical solution for the convergence of the tunnel walls as a function of two parameters, the distance to the face and the time. For a similar problem, a closed-form solution for the pressure acting on tunnel support structures was given by Sakurai (1978 and 1997). In this study, an attempt was made to develop new equations to generalize the Sulem et al. equations for a non-hydrostatic condition (biaxial stress field). However, similar to the Sulem et al. assumptions, it was assumed that the tunnel has a circular cross-section and around the tunnel, the rock is homogeneous and isotropic.

Seimare power tunnel, which was considered as a case study, is a part of the waterways system for the Seimare power station. The field data collected from the Seimare monitoring program was compared with the numerical analysis results as well as the proposed analytical solution results. The comparative results showed that the field data don't meet the numerical and analytical results, while the numerical and analytical results are very close together. However, it was expected such differences due to the existence of some construction activities adjacent to the monitoring stations. In addition, the initial data used in the numerical modelling and analytical analysis probably did not have enough accuracy as a representative of the rock within the selected stations.

6 ACKNOWLEDGEMENTS

I would like to express my sincere gratitude to Prof. Adolfo Foriero for his guidance and support throughout my work in this study. The field data of the Seimare power tunnel used in this paper has been provided by Iran Water & Power Resources Development Company (IWPCO). I would like also to appreciate them, especially their technical office at the dam site, for their friendly assistance and providing valuable data. The manuscript has been substantially improved by addressing the review comments from Dr. Farbod Saadat.

7 REFERENCES

Jaeger, J.C. and Cook, N.G., 1969. *Fundamentals of rock mechanics*, Methuen & Co. Ltd., London, UK.

Kirsch, E.G., 1898. The theory of elasticity and the need of the strength of materials (translated.). *Journal of the Association of German Engineers*, 42: 797-807.

Mahab Ghodss Consulting Engineering Company, 2003. *Rock mechanics reports of the Seimare power tunnel,* second phase study, Seimare Project, Iran.

Panet M., 1993. *Comprehensive Rock Engineering, Understanding deformations in tunnels,* Chapter 27, Vol. 1 (Fundamentals), Elsevier, USA.

Panet M., 1979. Time-dependent deformations in underground works, *proceeding of the 4th Congress of ISRM*, 279-289.

Sakurai S., 1997. Lessons learned from filed measurements in tunneling, *tunneling and Underground Space Technology*, 12(4): 453-460.

Sakurai S., 1978. Approximate time-dependent analysis of tunnel support structure considering progress of tunnel face, *International Journal for Numerical and Analytical Methods in Geomechanics*, 2: 159-175.

Sulem J., Panet M., and Guenot A., 1987. Closure Analysis in Deep Tunnels, *International Journal of Rock Mechanics and Mining Sciences & Geomechanics*, 24(3): 145-154.

Sulem J., Panet M., and Guenot A., 1987. An Analytical Solution for Time-dependent Displacements in a Circular Tunnel, *International Journal of Rock Mechanics and Mining Sciences & Geomechanics*, 24(3): 155-164.